Advances in Difference Equations
a SpringerOpen Journal

RESEARCH Open Access

Pattern self-organization and pattern transition on the route to chaos in a spatiotemporal discrete predator–prey system

Tousheng Huang, Xuebing Cong, Huayong Zhang*, Shengnan Ma and Ge Pan

*Correspondence:
rceens@ncepu.edu.cn
Research Center for Engineering Ecology and Nonlinear Science, North China Electric Power University, Beijing, P.R. China

Abstract

A spatiotemporal discrete predator–prey system is investigated for understanding the pattern self-organization on the route to chaos. The discrete system is modelled by a coupled map lattice and shows advection of populations in space. Based on the conditions of stable stationary states and Hopf bifurcation, Turing pattern formation conditions are determined. As the parameter value is changed, self-organization of diverse patterns and complex phase transition among the patterns on the route to chaos are observed in simulations. Ordered patterns of stripes, bands, circles, and various disordered states are revealed. When we zoom in to observe the pattern transition in smaller and smaller parameter ranges, subtle structures for transition process are found: (1) alternation between self-organized structured patterns and disordered states emerges as the main nonlinear characteristic; (2) when the parameter value varies in the level from 10^{-3} to 10^{-4}, a cyclic pattern transition process occurs repeatedly; (3) when the parameter value shifts in the level of 10^{-5} or below, stochastic pattern fluctuation dominates as essential regularity for pattern variations. The results obtained in this research promote comprehending pattern self-organization and pattern transition on the route to chaos in spatiotemporal predator–prey systems.

Keywords: Self-organization; Chaos; Coupled map lattice; Bifurcation; Turing instability; Predator–prey system

1 Introduction

In nature, the patterns are a type of non-uniform macroscopic structures with certain orderliness, and they exist commonly and widespreadly [1, 2], and [3]. After decades of research, pattern dynamics has become an important discipline widely applied in various fields [1, 2], and [4]. In the field of ecology, many researchers found that spatial pattern formation is one of the most basic nonlinear characteristics of ecological systems [5] and [6]. On the one hand, spatial composition of ecological relations is a key factor in determining formation and development of biological communities. For example, in predator–prey systems, the predator exerts effort to capture the prey; in turn, the prey strives to escape from the predator's hunt. With such predator–prey interactions expanding in space, the

dynamics and spatial distribution of predator and prey can be more accurately described [7]. On the other hand, spatial pattern formation presents a widespread existence in ecological systems and has attracted attention of many researchers [8]. For example, in arid and semi-arid areas, the plants are often self-organized into regular spatial patterns due to the competition for water resource. This has been verified by numerous field observations [9].

The investigation on spatial pattern formation in ecological systems extends the approach of temporal models and develops the temporal dynamics and stability to spatiotemporal scale. Since spatial patterns often exist in multi-levels and multi-scales of ecological systems, the pattern self-organization represents an important aspect of ecological complexity, i.e., spatiotemporal complexity [10]. Usually, such spatiotemporal complexity is manifested by pattern diversity, including spotted, striped, labyrinth, and spiral patterns, as well as many spatiotemporally chaotic patterns [3] and [8]. As research on pattern dynamics progressed, the researchers noticed that dynamical destabilization and corresponding pattern formation had similarities with equilibrium phase transition [11]. It was also found that the self-organization of spatial patterns plays a key role in indicating catastrophes in ecological systems [8]. Therefore, the study on spatial pattern formation demonstrates great significance in ecology.

In ecological systems, interactions between species are important features. Among the species interactions, predator–prey relationship is one of the most basic and widespread existing interactions. Since the predator–prey interactions always take place over a range of spatial and temporal scales, nonlinear interactions and spatial heterogeneity can often lead to spontaneous formation of predator–prey patterns [3]. During last four decades, spatial pattern formation in spatiotemporal predator–prey systems has received significant attention from many researchers [3, 12], and [13]. Based on the research of pattern self-organization in predator–prey systems, the comprehension of ecological spatiotemporal complexity is promoted.

Studies in mathematical models are informative in understanding the dynamic relationship between the predator and the prey and their complex properties [3] and [14]. For studying the pattern formation in predator–prey systems, a reaction–diffusion model is the most mainstream theoretical model, of which the nonlinear mechanism for pattern self-organization is known as Turing instability. In 1972, Segel and Jackson first applied reaction–diffusion model to study population dynamics: dissipative instability of the copepods–phytoplankton interactions [15]. In the same year, Gierer and Meinhardt explained the biological mechanism of a reaction–diffusion model and studied the properties of corresponding Turing patterns [16]. In 1976, Levin and Segel published a paper in *Nature*, suggesting that formation of Turing patterns may be the fundamental mechanism for plankton patchiness [17]. Based upon the classical works of Segel and Jackson [15] and Levin and Segel [16], intense research works have been performed to investigate the self-organization of predator–prey patterns due to diffusive instability, with the application of Turing's instability theory. The reaction–diffusion models have contributed to revealing and explaining the self-organization of various predator–prey patterns.

The reaction–diffusion models capture two basic nonlinear characteristics of reaction–diffusion systems, i.e., "reaction" between system variables and diffusion motion of the system variables in space [18]. With continuous development on the reaction–diffusion models, many researchers found that a different type of population motion, advection,

can be incorporated [19] and [20]. In predator–prey systems, advection implies that the spatial motion of population(s) has the characteristic of directional flow, i.e., the individuals exhibit a correlated motion towards certain direction [21] and [22]. One of the most typical advection motions may result from correlated motion caused by purely environmental factors such as wind in case of seeds spreading or water current in case of plankton communities [23]. In literature, a general predator–prey model incorporating advection and diffusion can be described by

$$\frac{\partial N}{\partial T} = F(N,P) + C_1\frac{\partial N}{\partial X} + D_1\left(\frac{\partial^2 N}{\partial X^2} + \frac{\partial^2 N}{\partial Y^2}\right), \tag{1a}$$

$$\frac{\partial P}{\partial T} = G(N,P) + C_2\frac{\partial P}{\partial X} + D_2\left(\frac{\partial^2 P}{\partial X^2} + \frac{\partial^2 P}{\partial Y^2}\right), \tag{1b}$$

in which N and P are the predator and the prey, respectively; T is time and X and Y give the two-dimensional space coordinates; $F(N,P)$ and $G(N,P)$ describe the temporal dynamics of the predator and prey; C_1 and C_2 are the advection rates, and D_1 and D_2 are the diffusion coefficients. The system described by Eqs. (1a)–(1b) can be called advection–reaction–diffusion predator–prey system. Liu [22] and Sun et al. [20] studied such systems, showing that advection has prominent effect on the pattern formation of the population, i.e., changing Turing pattern into traveling pattern. Via the investigation of Sun et al. [21], it is suggested that the combining effects of diffusion and advection can account for dynamical complexity of ecosystems.

Based on the reaction–diffusion model, a new model, coupled map lattice (CML), can be developed [24, 25], and [26]. The CML is a type of spatiotemporally discrete model widely applied in an ecological field. Since the pioneering work of May on the discrete logistic model [14], many studies have revealed that the discrete model can exhibit rich nonlinear dynamics for predator–prey systems [24, 27], and [28]. As is well known, flip bifurcation and Hopf bifurcation are the key for triggering the route to chaos, on which complex dynamical behaviors always emerge, such as periodic window, invariant cycles, and chaotic attractors. The research on the routes to chaos has contributed greatly to better comprehending the ordered and disordered states in predator–prey systems. Moreover, the transition between the ordered and disordered states becomes one of the most important topics and attracts the attention of many researchers [29] and [30]. Via comparison, the researchers have also found that CMLs are more practical in describing nonlinear characteristics and spatiotemporal complexity of predator–prey systems than the continuous reaction–diffusion model. With the application of CMLs, many new attractive results have been produced [12, 13, 18, 24, 25], and [26]. Rodrigues et al. [13] revealed a rich variety of pattern formation scenarios in a space- and time-discrete predator–prey system with strong Allee effect and found spatiotemporal multistability under the effects of different initial conditions. Huang et al. [12] and [18] compared the spatial pattern formation between the reaction–diffusion model and its CML version, demonstrating that the nonlinear mechanisms of CML better capture the dynamical complexity of the predator–prey systems. In particular, CMLs can depict discontinuous properties (e.g., patchy environment or fragmented habitat) of predator–prey systems [25]. By the nonlinear mechanisms of CMLs, the spatiotemporal complexity of predator–prey systems can be further revealed and profoundly understood [12, 25, 31], and [26].

In this research, the CML will be applied to investigate the spatiotemporal complexity of the advection–reaction–diffusion system described by Eqs. (1a)–(1b). In former research, Huang et al. have explored a reaction–diffusion predator–prey system with the same functional response, suggesting that such an investigation with discrete time variable and space variable would discover new nonlinear characteristics and dynamical complexity [12]. Extending the study of Huang et al. [12], this research further investigates two more aspects. First, the influence of advection on the spatiotemporal dynamics of a discrete predator–prey system is still limitedly known and therefore deserves investigation. Second, pattern self-organization and pattern transition on the route to chaos are an important topic which still shows challenge. The exploration in this research is arranged as follows. Section 2 gives the CML model and the basic nonlinear characteristics of the discrete predator–prey system. Section 3 performs the Turing instability analysis and determines the pattern formation conditions. Section 4 demonstrates the numerical simulations, and Sect. 5 provides discussion and conclusions.

2 CML model description and system characteristics

2.1 Description of the CML model

Huang et al. [12] have investigated the spatiotemporal complexity of a space- and time-discrete predator–prey system with Beddington–DeAngelis functional response. They found that the CML model can exhibit a surprising variety of spatiotemporal patterns, including regular and irregular patterns of spots, stripes, labyrinth, gaps, mosaics, spirals, circles, and many intermediate patterns in-between. Based on the research of Huang et al. [12], interest in three aspects is triggered. First, on the route to chaos induced by Hopf bifurcation, how the coupled effects of Turing instability and Hopf instability lead to the self-organization of complex patterns. Second, what are the results when spatial symmetry breaking occurs on the homogeneous chaotic oscillating states on the route to chaos. Third, how the dynamic transition occurs between ordered patterns and completely disordered states along the routes to chaos. With these interests, we still consider investigating the discrete Beddington–DeAngelis type predator–prey system in this research in order to further know how the pattern self-organization and pattern transition emerge on the route to chaos. Therefore, two functions F and G for determining the temporal dynamics of predator and prey are utilized:

$$F(N,P) = rN\left(1 - \frac{N}{K}\right) - \frac{\beta NP}{B + N + wP}, \tag{2a}$$

$$G(N,P) = \frac{\varepsilon\beta NP}{B + N + wP} - \eta P, \tag{2b}$$

where r stands for maximum per capita growth rate of the prey; K is the carrying capacity; β is the maximum consumption rate; B is a half-saturation constant; w is the predator interference parameter; ε is the conversion rate of eaten prey into new predator abundance; η is the per capita predator death rate. The logistic term in Eq. (2a) is used to describe the general prey growth. The Beddington–DeAngelis functional response, which is one of the most important functional responses in predator–prey systems and has been extensively investigated, describes the predation relationship with interference effects. Through many research works, it has been found that the Beddington–DeAngelis functional response is very important for the predator–prey systems exhibiting dynamical complexity

[32] and [31]. Especially, a predator–prey system with Beddington–DeAngelis functional response may generate various instability mechanisms, including Hopf–Turing instability, Pitchfork–Turing instability, Bogdanov–Takens–Turing instability, and so on [31].

For developing the CML model, a two-dimensional rectangular lattice divided into $n \times n$ sites by space interval h is considered. Simultaneously, the time is divided into a series of slices with time interval τ. Parameters τ and h are the time scale and the space scale for describing the predator–prey dynamics, respectively. Since the growth, death, feeding, and migration of predator and prey individuals always occur periodically, the dynamics of a predator–prey system can be observed by a particular time scale, which can be defined by the generation span of the predator and prey populations and measures the regeneration time of both populations. On the other hand, the space scale on which spatial movements of predator and prey take place can be defined by maximum size of dwelling sites of predator and prey individuals.

In such a spatiotemporal scale, two discrete state variables are defined as $N_{(i,j,m)}$ and $P_{(i,j,m)}$ $(i,j \in \{1,2,3,\dots,n\})$, which describes the prey density and the predator density in (i,j) site at mth iteration (notice that with initial time t_0, the time at mth iteration is $t_0 + m\tau$). The prey and predator densities in each site change with time in course of the system dynamics, due to the local inter- and intra-specific interactions as well as migration or dispersal between different sites [25].

According to the research works about CML [12] and [25], the dynamics from mth to m+1th iteration consists of two distinctly different stages, (a) the spatial movement stage and (b) the "reaction" stage. The spatial movement stage can be obtained by discretizing the spatial terms of Eqs. (1a)–(1b), i.e.,

$$\phi'_{(i,j,m)} = \phi_{(i,j,m)} + \frac{\tau}{h} C_k \nabla_{\mathrm{d}} \phi_{(i,j,m)} + \frac{\tau}{h^2} D_k \nabla_{\mathrm{d}}^2 \phi_{(i,j,m)}, \tag{3}$$

in which ϕ denotes the state variable of either N or P, $\phi'_{(i,j,m)}$ is the prey or predator density after advection and dispersal, C_k and D_k $(k = 1, 2)$ are the advection rate and the diffusion coefficient corresponding to the state variable ϕ as described in Eqs. (1a)–(1b), and ∇_{d} and ∇_{d}^2 are the discrete forms of advection operator and Laplacian operator, which can be described as

$$\nabla_{\mathrm{d}} \phi_{(i,j,m)} = \phi_{(i+1,j,m)} - \phi_{(i,j,m)}, \tag{4a}$$

$$\nabla_{\mathrm{d}}^2 \phi_{(i,j,m)} = \phi_{(i+1,j,m)} + \phi_{(i-1,j,m)} + \phi_{(i,j+1,m)} + \phi_{(i,j-1,m)} - 4\phi_{(i,j,m)}. \tag{4b}$$

The predator–prey reaction stage in the CML model can be expressed by the following equations:

$$N_{(i,j,m+1)} = f\left(N'_{(i,j,m)}, P'_{(i,j,m)}\right), \tag{5a}$$

$$P_{(i,j,m+1)} = g\left(N'_{(i,j,m)}, P'_{(i,j,m)}\right), \tag{5b}$$

where f and g are the functions determined by the local inter- and intra-specific interactions, and these two functions can be obtained via discretizing the non-spatial part of Eqs. (1a)–(1b) [12, 18], and [24], i.e.,

$$f(N,P) = N + \tau\left(rN\left(1 - \frac{N}{K}\right) - \frac{\beta NP}{B + N + wP}\right), \tag{6a}$$

$$g(N,P) = P + \tau\left(\frac{\varepsilon\beta NP}{B+N+wP} - \eta P\right). \tag{6b}$$

Noticing that spatial movement of populations always happens before the reaction stage at each iteration, combining Eqs. (3)–(6a)–(6b), we have

$$\begin{aligned} N_{(i,j,m+1)} = f\Bigg(& N_{(i,j,m)} + \frac{\tau}{h}C_k\nabla_{\mathrm{d}}N_{(i,j,m)} + \frac{\tau}{h^2}D_k\nabla_{\mathrm{d}}^2N_{(i,j,m)}, P_{(i,j,m)} \\ &+ \frac{\tau}{h}C_k\nabla_{\mathrm{d}}P_{(i,j,m)} + \frac{\tau}{h^2}D_k\nabla_{\mathrm{d}}^2P_{(i,j,m)}\Bigg), \end{aligned} \tag{7a}$$

$$\begin{aligned} P_{(i,j,m+1)} = g\Bigg(& N_{(i,j,m)} + \frac{\tau}{h}C_k\nabla_{\mathrm{d}}N_{(i,j,m)} + \frac{\tau}{h^2}D_k\nabla_{\mathrm{d}}^2N_{(i,j,m)}, P_{(i,j,m)} \\ &+ \frac{\tau}{h}C_k\nabla_{\mathrm{d}}P_{(i,j,m)} + \frac{\tau}{h^2}D_k\nabla_{\mathrm{d}}^2P_{(i,j,m)}\Bigg), \end{aligned} \tag{7b}$$

which gives a description of the CML model and describes a spatiotemporally discrete advection–reaction–diffusion predator–prey system with Beddington–DeAngelis functional response. From the ecological point of view, all the parameters involved in the CML model are positive and the values of $\phi_{(i,j,t)}$ are nonnegative. Moreover, for ensuring the nonnegativity of N and P, the parameter values should be provided to make $\tau C_k/h$ and $\tau D_k/h^2$ $(i = 1, 2)$ less than 0.5, based on the research of Huang et al. [12]. For applying the CML model, we set periodic boundary conditions as follows:

$$\phi_{(i,0,m)} = \phi_{(i,n,m)}, \qquad \phi_{(i,1,m)} = \phi_{(i,n+1,m)}, \qquad \phi_{(0,j,m)} = \phi_{(n,j,m)}, \qquad \phi_{(1,j,m)} = \phi_{(n+1,j,m)}.$$

2.2 Non-spatial dynamic characteristics of the discrete system

The non-spatial dynamics of the discrete system means no consideration of the advection and diffusion in the above CML model. Actually, the discrete system satisfies

$$\nabla_{\mathrm{d}}\phi_{(i,j,t)} = 0 \quad \text{and} \quad \nabla_{\mathrm{d}}^2\phi_{(i,j,t)} = 0. \tag{8}$$

Therefore, the non-spatial dynamics also reveals the spatially homogeneous states of the discrete system. Substituting Eq. (8) into the CML model, the non-spatial dynamics of the discrete system can be described by the following map:

$$\begin{pmatrix} N \\ P \end{pmatrix} \to \begin{pmatrix} N + \tau(rN(1-\frac{N}{K}) - \frac{\beta NP}{B+N+wP}) \\ P + \tau(\frac{\varepsilon\beta NP}{B+N+wP} - \eta P) \end{pmatrix}. \tag{9}$$

The above map (9) has been investigated in detail by Huang et al. [12]. Hereinafter, we just present the main results of the map. Firstly, the fixed points of map (9) are described as follows:

$$\begin{aligned} &(N_0, P_0) : (0,0); \qquad (N_1, P_1) : (K, 0); \\ &(N_2, P_2) : \left(\frac{K}{2rw\varepsilon}C, \frac{K(\beta\varepsilon-\eta)}{2rw^2\varepsilon\eta}C - \frac{B}{w}\right), \end{aligned} \tag{10}$$

in which $C = rw\varepsilon - \beta\varepsilon + \eta + \sqrt{(rw\varepsilon - \beta\varepsilon + \eta)^2 + \frac{4rwB\varepsilon\eta}{K}}$.

The stability of these fixed points was analyzed via the method of Jacobian matrix. According to the research of Huang et al. [12], we have

(1) (N_0, P_0) is unstable regardless of the parameter variations;
(2) when $0 < r\tau < 2$ and $\frac{\beta\varepsilon K}{B+K} < \eta < \frac{2}{\tau} + \frac{\beta\varepsilon K}{B+K}$, (N_1, P_1) is stable;
(3) (N_2, P_2) is stable when

$$a_{11}a_{22} - a_{12}a_{21} < 1, \qquad |a_{11} + a_{22}| < 1 + a_{11}a_{22} - a_{12}a_{21}, \tag{11}$$

in which

$$a_{11} = 1 + r\tau\left(1 - \frac{2N_2}{K}\right) - \frac{a_{21}}{\varepsilon}, \qquad a_{12} = -\frac{\tau\eta^2}{\beta\varepsilon^2}\left(1 + \frac{B}{N_2}\right),$$
$$a_{21} = \frac{r^2\tau\varepsilon}{\beta}\left(w + \frac{B}{P_2}\right)\left(1 - \frac{N_2}{K}\right)^2, \qquad a_{22} = 1 - \tau\eta - a_{12}\varepsilon.$$

Moreover, through bifurcation analysis on map (9), by applying the Hopf bifurcation theorem, Huang et al. [12] found that the discrete system undergoes supercritical Hopf bifurcation if the following conditions are satisfied:

$$\begin{aligned}
&(a_{11} - a_{22})^2 + 4a_{12}a_{21} < 0, \qquad a_{11}a_{22} - a_{12}a_{21} = 1,\\
&\frac{\beta\tau_0(1 - w\varepsilon)N_2P_2}{(B + N_2 + wP_2)^2} - \frac{r\tau_0N_2}{K} \neq -3, -2,\\
&d = \frac{rN_2}{2K^2\beta P_2}\left(K\beta P + r(w\varepsilon - 1)(K - N_2)^2\right) > 0,\\
&a = -\operatorname{Re}\left(\frac{(1 - 2\bar{\lambda})\bar{\lambda}^2}{1 - \lambda}\xi_{11}\xi_{20}\right) - \frac{1}{2}|\xi_{11}|^2 - |\xi_{02}|^2 + \operatorname{Re}(\bar{\lambda}\xi_{21}) < 0.
\end{aligned} \tag{12}$$

For detailed expressions of the above conditions, one can refer to Huang et al. [12].

Each fixed point of map (9) is exactly equivalent to a homogeneous stationary state of the discrete system. Therefore, (N_2, P_2) can represent a stable spatially homogeneous stationary state. Moreover, when supercritical Hopf bifurcation occurs, attracting invariant closed curves will emerge in the discrete system, representing the spatially homogeneous oscillating states.

3 Turing instability analysis and pattern formation conditions

Turing instability occurs when spatial symmetry breaking takes place and results in the change from spatially homogeneous states to Turing patterns. According to the previous description, the discrete system has two types of homogeneous states: homogeneous stationary state and homogeneous oscillating state. Turing instability occurring on the homogeneous stationary state is generally called pure Turing instability; Turing instability occurring on the homogeneous oscillating state often comes along with Hopf instability and therefore is called Hopf–Turing instability [12] and [18]. Under the influence of Turing instability, local spatially heterogeneous perturbations on the stable homogeneous states can gradually expand to the global spatial domain.

Spatially heterogeneous perturbations are introduced to perform the Turing instability analysis. Applying such perturbations to perturb the stable homogeneous stationary state

(N_2, P_2) gives

$$N_{(i,j,m)} = N_2 + \tilde{N}_{(i,j,m)}, \qquad P_{(i,j,m)} = P_2 + \tilde{P}_{(i,j,m)}, \tag{13}$$

where $\tilde{N}_{(i,j,m)}$ and $\tilde{P}_{(i,j,m)}$ are the perturbations on prey density and predator density in ijth site at mth iteration. Simultaneously, it should be noticed that

$$\nabla_{\mathrm{d}}\phi_{(i,j,m)} = \nabla_{\mathrm{d}}\tilde{\phi}_{(i,j,m)}, \qquad \nabla_{\mathrm{d}}^2\phi_{(i,j,m)} = \nabla_{\mathrm{d}}^2\tilde{\phi}_{(i,j,m)}. \tag{14}$$

Substituting Eqs. (13) and (14) into the equations of the CML model, we get

$$\begin{aligned}\tilde{N}_{(i,j,m+1)} &= a_{11}\left(\tilde{N}_{(i,j,m)} + \frac{\tau}{h}C_1\nabla_{\mathrm{d}}\tilde{N}_{(i,j,m)} + \frac{\tau}{h^2}D_1\nabla_{\mathrm{d}}^2\tilde{N}_{(i,j,m)}\right)\\ &\quad + a_{12}\left(\tilde{P}_{(i,j,m)} + \frac{\tau}{h}C_2\nabla_{\mathrm{d}}\tilde{P}_{(i,j,m)} + \frac{\tau}{h^2}D_2\nabla_{\mathrm{d}}^2\tilde{P}_{(i,j,m)}\right) + O^2, \end{aligned}\tag{15a}$$

$$\begin{aligned}\tilde{P}_{(i,j,m+1)} &= a_{21}\left(\tilde{N}_{(i,j,m)} + \frac{\tau}{h}C_1\nabla_{\mathrm{d}}\tilde{N}_{(i,j,m)} + \frac{\tau}{h^2}D_1\nabla_{\mathrm{d}}^2\tilde{N}_{(i,j,m)}\right)\\ &\quad + a_{22}\left(\tilde{P}_{(i,j,m)} + \frac{\tau}{h}C_2\nabla_{\mathrm{d}}\tilde{P}_{(i,j,m)} + \frac{\tau}{h^2}D_2\nabla_{\mathrm{d}}^2\tilde{P}_{(i,j,m)}\right) + O^2, \end{aligned}\tag{15b}$$

in which O^2 stands for a polynomial function with order at least two in the variables of $|\tilde{N}_{(i,j,m)}|$ and $|\tilde{P}_{(i,j,m)}|$. When the perturbations are small, O^2 can be ignored. Before we go to the next step of calculation on Eqs. (15a)–(15b), the eigenvalues of operators ∇_{d} and ∇_{d}^2 should be determined. Consider the following equations:

$$\nabla_{\mathrm{d}}X^{ij} + \lambda^{(1)}X^{ij} = 0, \tag{16a}$$

$$\nabla_{\mathrm{d}}^2Y^{ij} + \lambda^{(2)}Y^{ij} = 0, \tag{16b}$$

with periodic boundary conditions. Using the method described in Bai and Zhang [33], the eigenvalues of the two operators can be solved and described as follows:

$$\lambda_{kl}^{(1)} = 2\sin\phi_k \exp\left(\left(\phi_k - \frac{\pi}{2}\right)i'\right), \tag{17a}$$

$$\lambda_{kl}^{(2)} = 4\left(\sin^2\phi_k + \sin^2\phi_l\right), \tag{17b}$$

in which $\phi_k = \frac{(k-1)\pi}{n}$, $\phi_l = \frac{(l-1)\pi}{n}$, $i' = \sqrt{-1}$, and $k, l \in \{1, 2, 3, \ldots, n\}$. Simultaneously, one can verify that ∇_{d}^2 and ∇_{d} are commuting operators. Hence, a common set of eigenfunctions exists for both operators. Let X_{kl}^{ij} be the common eigenfunction of the eigenvalues $\lambda_{kl}^{(1)}$ and $\lambda_{kl}^{(2)}$. Applying X_{kl}^{ij} to multiply Eqs. (15a)–(15b) gives

$$\begin{aligned}\tilde{N}_{(i,j,m+1)} &= a_{11}X_{kl}^{ij}\tilde{N}_{(i,j,m)} + a_{12}X_{kl}^{ij}\tilde{P}_{(i,j,m)} + \frac{\tau}{h}a_{11}C_1X_{kl}^{ij}\nabla_{\mathrm{d}}\tilde{N}_{(i,j,m)} + \frac{\tau}{h}a_{12}C_2X_{kl}^{ij}\nabla_{\mathrm{d}}\tilde{P}_{(i,j,m)}\\ &\quad + \frac{\tau}{h^2}a_{11}D_1X_{kl}^{ij}\nabla_{\mathrm{d}}^2\tilde{N}_{(i,j,m)} + \frac{\tau}{h^2}a_{12}D_2X_{kl}^{ij}\nabla_{\mathrm{d}}^2\tilde{P}_{(i,j,m)} + O^2, \end{aligned}\tag{18a}$$

$$\begin{aligned}\tilde{P}_{(i,j,m+1)} &= a_{21}X_{kl}^{ij}\tilde{N}_{(i,j,m)} + a_{22}X_{kl}^{ij}\tilde{P}_{(i,j,m)} + \frac{\tau}{h}a_{21}C_1X_{kl}^{ij}\nabla_{\mathrm{d}}\tilde{N}_{(i,j,m)} + \frac{\tau}{h}a_{22}C_2X_{kl}^{ij}\nabla_{\mathrm{d}}\tilde{P}_{(i,j,m)}\\ &\quad + \frac{\tau}{h^2}a_{21}D_1X_{kl}^{ij}\nabla_{\mathrm{d}}^2\tilde{N}_{(i,j,m)} + \frac{\tau}{h^2}a_{22}D_2X_{kl}^{ij}\nabla_{\mathrm{d}}^2\tilde{P}_{(i,j,m)} + O^2. \end{aligned}\tag{18b}$$

Summing Eqs. (18a)–(18b) for all of ij and defining

$$\bar{N}_m = \sum_{i,j=1}^{n} X_{kl}^{ij} \tilde{N}_{(i,j,m)}, \qquad \bar{P}_m = \sum_{i,j=1}^{n} X_{kl}^{ij} \tilde{P}_{(i,j,m)}, \tag{19}$$

we can get the following transformed equations under the periodic boundary conditions [34]:

$$\begin{aligned} \bar{N}_{m+1} &= a_{11}\left(1 - \frac{\tau}{h} C_1 \lambda_{kl}^{(1)} - \frac{\tau}{h^2} D_1 \lambda_{kl}^{(2)}\right) \bar{N}_m \\ &\quad + a_{12}\left(1 - \frac{\tau}{h} C_2 \lambda_{kl}^{(1)} - \frac{\tau}{h^2} D_2 \lambda_{kl}^{(2)}\right) \bar{P}_m + \bar{O}^2, \end{aligned} \tag{20a}$$

$$\begin{aligned} \bar{P}_{m+1} &= a_{21}\left(1 - \frac{\tau}{h} C_1 \lambda_{kl}^{(1)} - \frac{\tau}{h^2} D_1 \lambda_{kl}^{(2)}\right) \bar{N}_m \\ &\quad + a_{22}\left(1 - \frac{\tau}{h} C_2 \lambda_{kl}^{(1)} - \frac{\tau}{h^2} D_2 \lambda_{kl}^{(2)}\right) \bar{P}_m + \bar{O}^2. \end{aligned} \tag{20b}$$

Similarly, $\bar{O}^2$ is a polynomial function with order at least two in the variables of $|\bar{N}_m|$ and $|\bar{P}_m|$.

According to the research work in literature, when one of the two eigenvalues of dynamic equations (20a)–(20b) is larger than one, the local heterogeneous perturbations introduced in (13) can diverge to the global spatial domain and lead to the formation of Turing patterns. Easily, the Jacobian matrix of linear dynamic equations (20a)–(20b) is found as

$$J = \begin{bmatrix} a_{11}(1 - \frac{\tau}{h} C_1 \lambda_{kl}^{(1)} - \frac{\tau}{h^2} D_1 \lambda_{kl}^{(2)}) & a_{12}(1 - \frac{\tau}{h} C_2 \lambda_{kl}^{(1)} - \frac{\tau}{h^2} D_2 \lambda_{kl}^{(2)}) \\ a_{21}(1 - \frac{\tau}{h} C_1 \lambda_{kl}^{(1)} - \frac{\tau}{h^2} D_1 \lambda_{kl}^{(2)}) & a_{22}(1 - \frac{\tau}{h} C_2 \lambda_{kl}^{(1)} - \frac{\tau}{h^2} D_2 \lambda_{kl}^{(2)}) \end{bmatrix}, \tag{21}$$

and the two eigenvalues of (21) can be calculated as

$$\lambda_{\pm}(k,l) = \frac{1}{2}\operatorname{tr}(J) \pm \frac{1}{2}\sqrt{\operatorname{tr}(J)^2 - 4\det(J)}, \tag{22}$$

where $\operatorname{tr}(J)$ and $\det(J)$ are the trace and determinant of Jacobian matrix (21). If we take one group of kl to make the maximum value of $\lambda_{\pm}(k,l)$ larger than one, divergence of perturbations takes place. Define

$$\lambda_m = \max_{k=1}^{n} \max_{l=1}^{n} \max\left(\left|\lambda_+(k,l)\right|, \left|\lambda_-(k,l)\right|\right), \tag{23}$$

and when

$$\lambda_m > 1, \tag{24}$$

Turing instability emerges in the discrete system and the self-organization of Turing patterns can be observed.

4 Numerical simulations

Simulations are carried out to exhibit the spatiotemporal dynamics of the discrete system. Based on the calculations in Sect. 3, parametric conditions for numerical simulations can be provided. Combining with the research of Huang et al. [12], the values of the following parameters can be fixed as $\beta = 0.6$, $\varepsilon = 1$, $B = 0.4$, $w = 0.4$, $\eta = 0.25$, $K = 1.8$, and $r = 0.8$. Simultaneously, we can choose $C_1 = 0.1$, $C_2 = 0.01$, $D_1 = 0.01$, $D_2 = 0.1$, $h = 10$, and $n = 100$, and shift the value of parameter τ to observe the dynamical variations of the discrete system.

Figure 1 demonstrates the change of dynamical characterizations as the value of parameter τ grows. With the parametric conditions given as $r = 0.8$, $K = 1.8$, $\beta = 0.6$, $\varepsilon = 1$, $B = 0.4$, $w = 0.4$, $\eta = 0.25$, the Hopf bifurcation point of the discrete system can be determined at about $\tau_0 = 3.0714$ (Fig. 1(a)). Simultaneously, we can verify that at the critical bifurcation point, $\lambda_{1,2} = 0.7352 \pm 0.6778i'$ and $|\lambda_{1,2}| = 1$. The values of γ and a_0 are determined as $d = 0.0862$ and $a = -0.5024$. Since $d > 0$ and $a < 0$, based on the conditions for Hopf bifurcation provided in Sect. 2, we know that when $\tau < \tau_0$, a stable fixed point takes place in the N–P state space, and that when $\tau \geq \tau_0$, the fixed point turns to be unstable and the dynamics of the discrete system is attracted to an invariant closed curve. Moreover, the Hopf bifurcation starts a route to chaos, in which periodic windows repeatedly occur.

As demonstrated in Fig. 1(b), it can be found that the discrete system enters a chaotic dynamics zone at about $\tau = 4.2243$ from the maximum Lyapunov exponent larger than one. Fig. 1(c) exhibits the variation of the value of λ_m, determining the range of τ for occurrence of Turing instability. Explicitly via $\lambda_m = 1$, the threshold value for Turing instability occur-

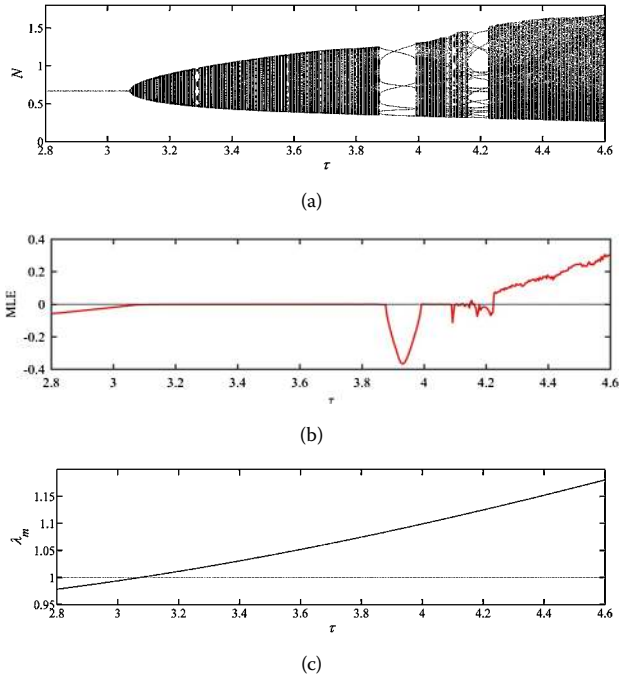

Figure 1 Diagrams of (**a**) Hopf bifurcation, (**b**) maximum Lyapunov exponent (MLE), and (**c**) λ_m, demonstrating the change of dynamical properties of the discrete system corresponding to variation of parameter τ. $r = 0.8$, $K = 1.8$, $\beta = 0.6$, $\varepsilon = 1$, $B = 0.4$, $w = 0.4$, $\eta = 0.25$, $C_1 = 0.1$, $C_2 = 0.01$, $D_1 = 0.01$, $D_2 = 0.1$, $h = 10$, and $n = 100$

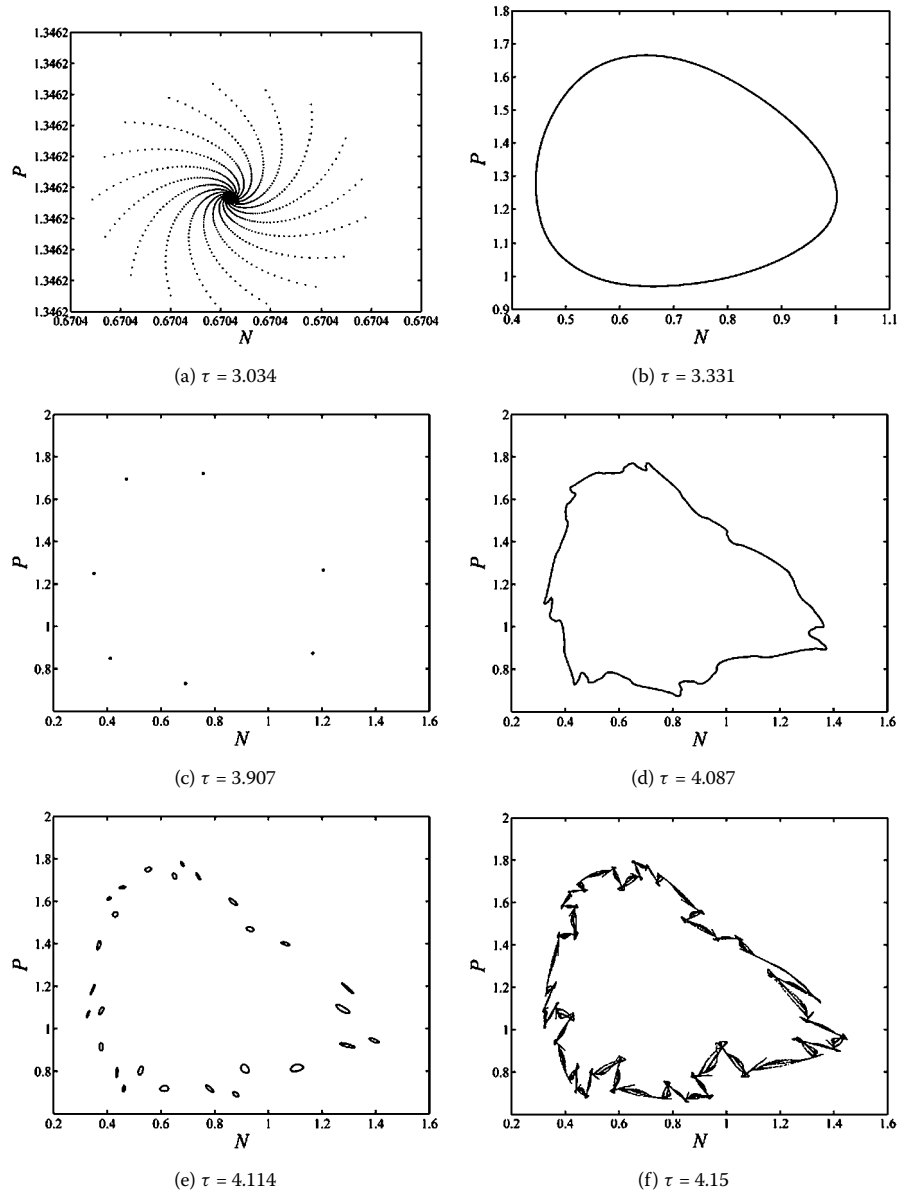

Figure 2 Phase diagrams corresponding to the bifurcation diagram in Fig. 1(a), demonstrating the dynamic transition on the route to chaos induced by the Hopf bifurcation

rence is at about $\tau = 3.0714$. This suggests the overlap of a Hopf bifurcation point and a Turing bifurcation point, forming the Hopf–Turing bifurcation point. When the value of parameter τ is larger than the Hopf–Turing bifurcation point, the occurrence of Turing instability along the route to chaos can bring the formation of Turing patterns.

Figure 2 exhibits different dynamic behaviors in the N–P state space corresponding to the bifurcation diagram. Fig. 2(a) shows a stable fixed point, which is a focus. Over the Hopf bifurcation point, an attracting closed curve appears in the state space (Fig. 2(b)). And then, as the value of parameter τ continuously rises, the transition of predator–prey dynamics in the state space sequentially experiences from period-7 orbit (Fig. 2(c)), to complex invariant closed cycles (Fig. 2(d)–(f)), then to period-20 orbit (Fig. 2(g)), and

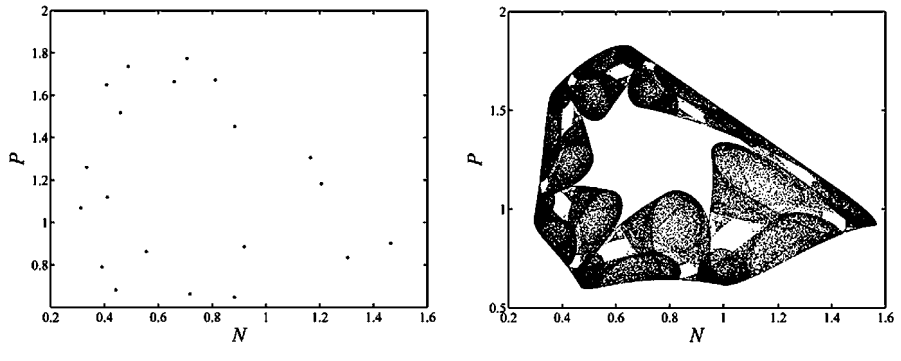

(g) $\tau = 4.222$

(h) $\tau = 4.285$

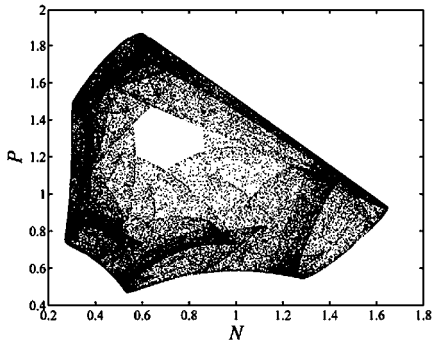

(i) $\tau = 4.528$

Figure 2 Continued

finally to chaotic attractors (Fig. 2(h)–(i)). In the discrete system, the periodic orbit, invariant closed cycles, and chaotic attractors correspond to different states that are homogeneous in space and periodic, quasiperiodic, and chaotic oscillating in time, respectively. Turing instability induces spatial symmetry breaking on these states. Therefore, diversity and complexity of the pattern self-organization in the discrete system may be exhibited.

Pattern formation simulations are then performed. In this research, initial conditions for pattern formation simulations are provided as follows:

$$N = N_2(1 + \xi) + 0.05, \tag{25a}$$

$$P = P_2(1 + \xi) + 0.05, \tag{25b}$$

where ξ is a random variable uniformly distributed in $(-0.05, 0.05)$. Under Hopf–Turing instability mechanism, the pattern formation process is very sensitive to initial conditions [12] and [18]. For comparing the self-organized patterns on the route to chaos induced by the Hopf bifurcation, initial conditions with the same random perturbations as described in (25a)–(25b) are applied for all pattern simulations. On the other hand, the patterns self-organized on the route to chaos also show oscillating property with time. Therefore, transient states of predator and prey at large evolution time are chosen for displaying such pattern formation. The choice of large evolution time needs avoiding the influence of initial pattern evolution process. Through a great number of pattern simulations, a large evolution time such as $t = 20{,}000$ would satisfy this condition. Furthermore, parametric

conditions for pattern simulations are given the same as those in Fig. 1, and the value of parameter τ ranges in $[2.8, 4.6]$. The advection direction in each pattern graph is set from up to down. Since predator and prey patterns always show similar configuration, we here only demonstrate the prey pattern. Lastly, it should be noticed that exactly the same simulation conditions are utilized for all simulations, except the change of τ value, for the purpose of pattern comparison.

With a large amount of numerical simulations, we find that the discrete system often presents two counter types of heterogeneous states. The first type holds distinguishable self-organized ordered structures in configuration, such as circles, stripes, and lines. This type of heterogeneous states is called ordered patterns in this research. Nevertheless, for another type, the spatial distribution of population density is so irregular, scattered, or chaotic that we can hardly visually recognize any ordered structures in the configuration. Therefore, we named the second type of heterogeneous states disordered states hereinafter.

Moreover, we still choose the parameter τ as the main variable inducing pattern transition on the route to chaos. Mathematically, this parameter shows an equal role to other parameters in the discrete system, which can be also chosen to make similar demonstration. From ecology point of view, parameter τ measures the time scale on which predator–prey dynamics takes place, including the growth, death, predating, feeding, and migration of predator and prey individuals, and can be defined by the generation span of the predator and prey populations. With the change of this parameter, we find that the population regeneration is important for determining the spatiotemporal predator–prey dynamics. In literature, this parameter has been also used to explore the dynamic transition from periodic to chaotic behaviors on the route to chaos [27] and [28]. The values of parameters C_1, C_2, D_1, and D_2 are best to range in $(0, 1]$, in which the variation of these parameters may hardly change the trend of pattern transition. Based on the numerical simulations, variation of these parameters mainly controls the configuration and occurrence range of striped patterns.

In order to investigate the pattern transition in the range $[2.8, 4.6]$, the range is divided into 50 segments and pattern simulations are carried out at each segmentation point. Figure 3 shows the transition process with main types of prey patterns. At the beginning, the

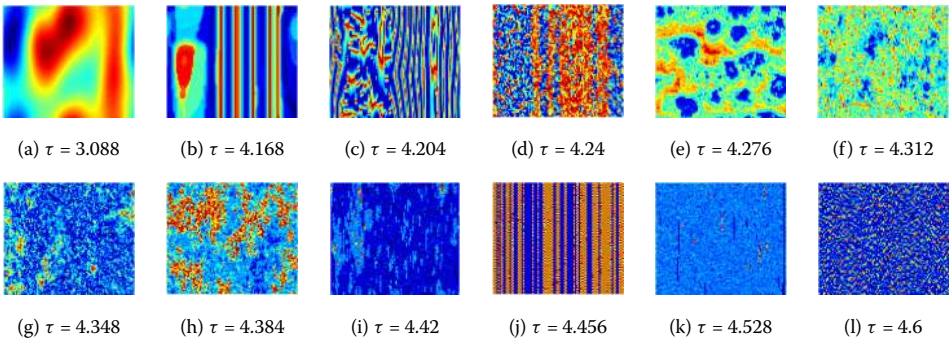

Figure 3 Pattern self-organization and transition on the route to chaos with the variation of τ covering $[2.8, 4.6]$. $t = 20{,}000$, the parametric conditions are the same as those in Fig. 1. The initial conditions are given by (25a)–(25b) and are exactly the same for each pattern graph. The advection direction is from up to down. These conditions are also the same for all the pattern simulations hereinafter

dynamics of the discrete system is dominated by homogeneous and approximately homogeneous states until the τ value is larger than 4.132 (see Fig. 3(a)). Then the striped pattern emerges suddenly, with striped patches parallel to the advection direction (see Fig. 3(b)). After the transition of intermediate patterns (Fig. 3(c)–(d)), the striped pattern gradually changes to disordered states in which the prey patches distribute irregularly (Fig. 3(e)–(i) and 3(k)–(l)). Nevertheless, the discrete system may return to the striped pattern in between the disordered states.

To quantitatively determine the regularity of pattern transition along the route to chaos, three aspects of pattern characterizations are utilized.

(a) Mean value of N pattern (MVN), defined as

$$\mathrm{MVN} = \sum_{i=1}^{i=n} \sum_{j=1}^{j=n} N(i,j,t) \Big/ n^2. \tag{26}$$

(b) Main states of N pattern (MSN), defined as

$$\mathrm{MSN} = \left\{ N(i,j,t) | \, \mathrm{pos}\big(N(i,j,t)\big) \geq 0.001 \right\}, \tag{27}$$

in which $\mathrm{pos}(N(i,j,t))$ represents the occurrence possibility of the state $N(i,j,t)$ in the prey pattern. To exhibit the main states of the pattern, we need to remove the states of very low occurrence possibility (such as 0.001). With the given n value as 100, $\mathrm{pos}(N(i,j,t)) = 0.001$ means the occurrence frequency of $N(i,j,t)$ equals 10. Hence, MSN does not contain the states with occurrence frequency less than 10.

(c) Information entropy of N pattern (IEN), defined as

$$\mathrm{IEN} = -\sum \mathrm{pos}\big(N(i,j,t)\big) \log\big(\mathrm{pos}\big(N(i,j,t)\big)\big). \tag{28}$$

The graphs of MVN, MSN, and IEN in Fig. 4 demonstrate a general trend of pattern transition as the parameter τ ranges in $[2.8, 4.6]$. When the τ value crosses the Hopf–Turing bifurcation point, the following dynamic characteristics can be described. First, the change of MVN is sensitive to parameter variation and presents large fluctuation. Correspondingly, in Fig. 4(a), the distribution exhibits an appearance of point cloud. Second, two types of patterns can be distinguished from the MSN as shown in Fig. 4(b). One has low number and discontinuous main states, which also fluctuate around the MVN. In such a case, homogeneous states, approximately homogeneous states, or simple two-phase heterogeneous patterns may be dominant. The other has large numbers and continuous main states, and complex and diverse patterns prevail. The dividing point of these two types of patterns is at about $\tau = 4.1572$. Compared with the bifurcation diagram, the non-spatial dynamics of the discrete system at this dividing point is just the beginning of the periodic window, after which chaotic dynamics sequentially follows. Third, the above dividing point is also the key for the change of IEN (Fig. 4(c)). Before the dividing point, IEN shows low values. It should be noticed that IEN equal to zero corresponds to homogenous states. Therefore, Fig. 4(c) demonstrates the alternation between homogeneous states and heterogeneous patterns in the range of $[3.0714, 4.1572]$. After the diving point, IEN has large values. Compared with Fig. 3, we find that large IEN implies the self-organization of complex and diverse patterns.

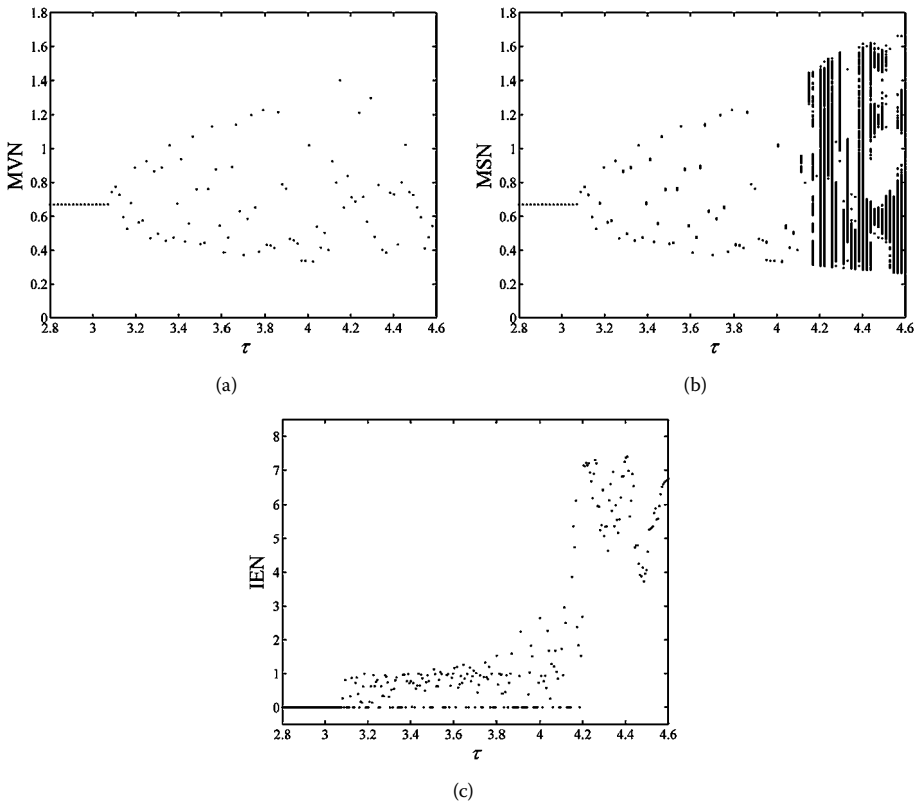

Figure 4 Graphs of (**a**) MVN, (**b**) MSN, and (**c**) IEN corresponding to Fig. 3, demonstrating the general trend of pattern transition on the route to chaos with parameter τ ranging in [2.8, 4.6]

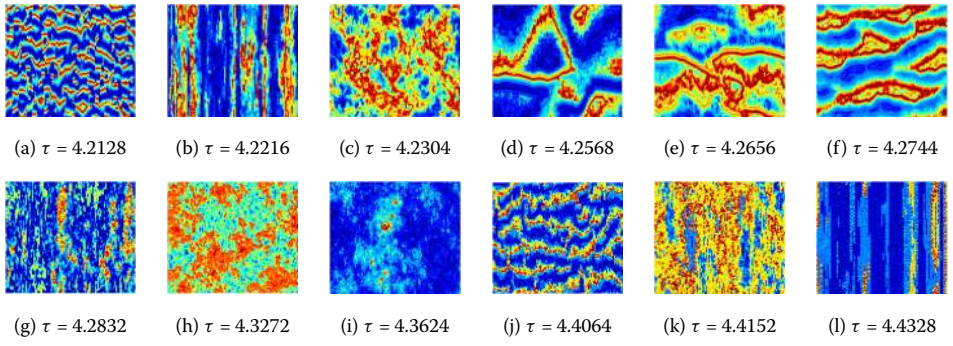

Figure 5 Pattern self-organization and transition with τ value ranging in [4.16, 4.44]. Various striped patterns, circled patterns, and disordered patterns are demonstrated. The conditions for pattern simulations are exactly the same as those in Fig. 3

To further reveal the spatiotemporal complexity and dynamic variation on the route to chaos, we zoom in to observe the self-organization of patterns and pattern transition in the range [4.16, 4.44]. We also divide this range into 50 segments and then perform the pattern formation simulations. In Fig. 5, different striped patterns as well as a circled pattern are demonstrated. The stripes in the striped patterns may be parallel or perpendicular to the advection direction (Fig. 5(a), 5(b), and 5(g)). Especially, the stripes can reach and combine with each other and lead to the self-organization of a circular struc-

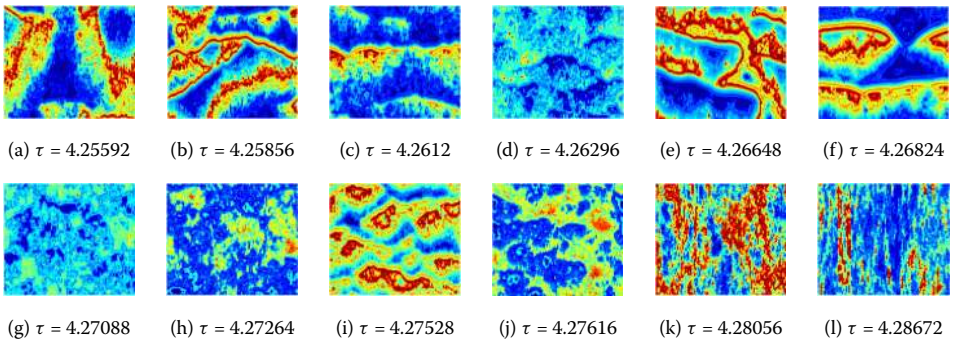

Figure 6 Pattern self-organization and transition with τ value ranging in [4.248, 4.292]. Alternation between self-organized structured patterns and disordered states is shown in this range. The conditions for pattern simulations are exactly the same as those in Fig. 3

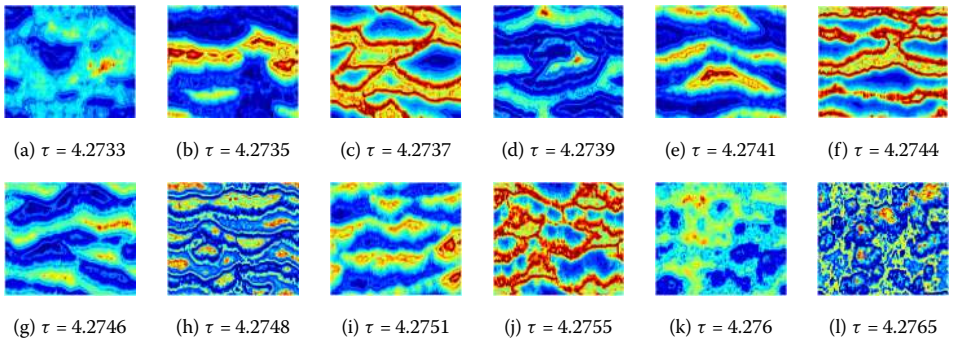

Figure 7 Pattern self-organization and transition with τ value ranging in [4.272, 4.277]. Cyclic transitions of patterns are found in the alternation between ordered patterns and disordered states. The conditions for pattern simulations are exactly the same as those in Fig. 3

ture (Fig. 5(d)). Moreover, direct combination of two or several stripes may result in the formation of wide bands in the pattern (Fig. 5(f)). In between these patterns which have explicit self-organized structures, disordered states repeatedly emerge (such as Fig. 5(c), 5(h), and 5(k)).

When we further zoom in to investigate the pattern self-organization on the route to chaos, we find that the alternation between self-organized structured patterns and disordered states also takes place in a smaller parameter range, such as in the range [4.248, 4.292] (see Fig. 6). Such alternation reveals that the ordered and disordered states of the discrete system can keep in continuous transition from one to the other. However, the regularity of the alternation is implicit. Only further zooming in on smaller parameter ranges (see Figs. 7 and 8), we find interesting phenomena of dynamic variation: the alternation between ordered patterns and disordered states results from many cyclic transitions of patterns. As shown in Fig. 7, the cyclic transition process occurs repeatedly in the range [4.272, 4.277]. Figure 8 illustrates the detailed information of the cyclic transition process as the value of parameter τ increases in [4.2734, 4.2739]: at first, the pattern is disordered with low prey density (Fig. 8(a)); gradually, a few circles and bands just "grow" from the disordered background (Fig. 8(b)–8(d)); the emerging circles and bands may combine together, leading to the self-organization of pattern structures (Fig. 8(e)–8(h)); as τ value

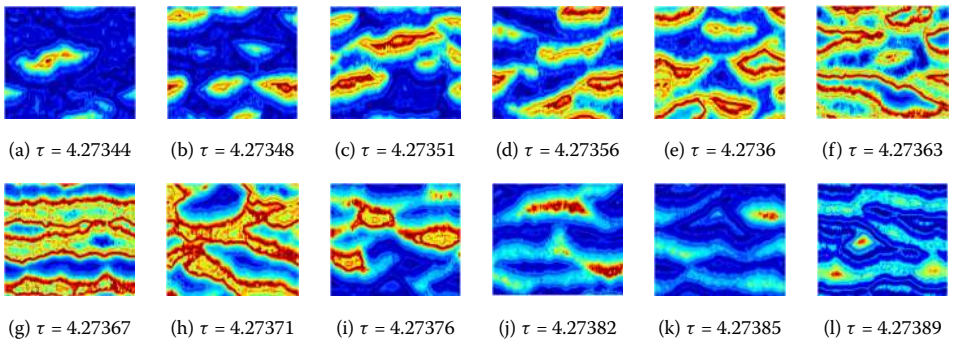

(a) $\tau = 4.27344$ (b) $\tau = 4.27348$ (c) $\tau = 4.27351$ (d) $\tau = 4.27356$ (e) $\tau = 4.2736$ (f) $\tau = 4.27363$

(g) $\tau = 4.27367$ (h) $\tau = 4.27371$ (i) $\tau = 4.27376$ (j) $\tau = 4.27382$ (k) $\tau = 4.27385$ (l) $\tau = 4.27389$

Figure 8 Pattern transition with the variation of τ covering [4.2734, 4.2739]. Detailed information of the cyclic transition process in Fig. 7 is shown. The conditions for pattern simulations are exactly the same as those in Fig. 3

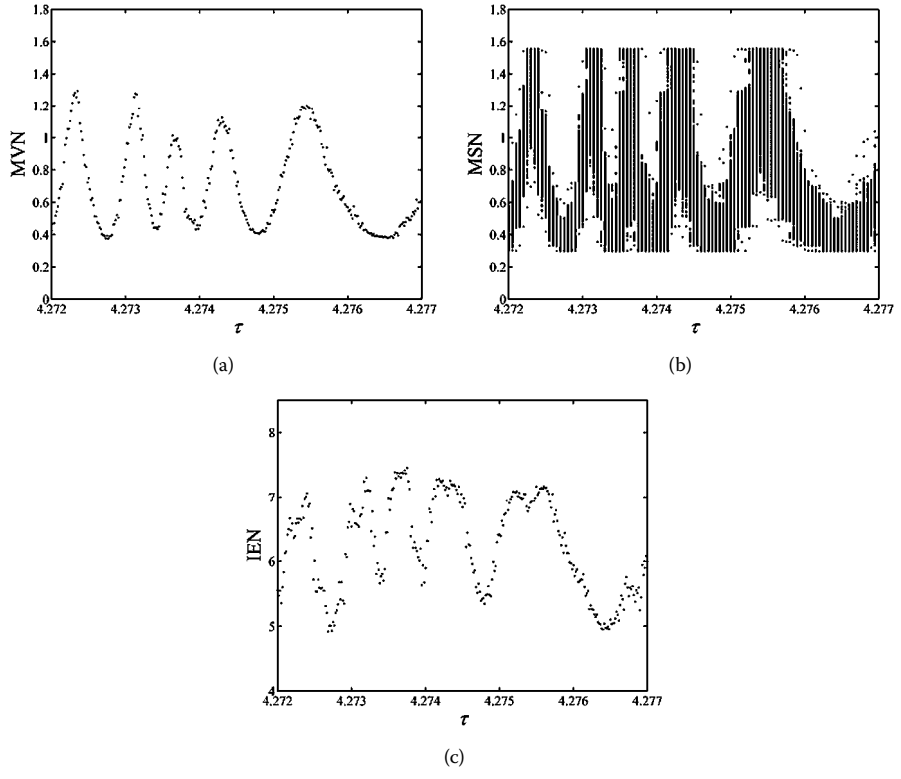

(a) (b)

(c)

Figure 9 Graphs of (**a**) MVN, (**b**) MSN, and (**c**) IEN corresponding to Fig. 7. The waved variations of MVN, MSN, and IEN explicitly display the cyclic pattern transition process in Fig. 7

further rises, the above process will go through in a reversed way, i.e., the pattern structures decompose, then circles and bands disappear, and finally disordered states dominate again (Fig. 8(i)–8(l)). The cyclic pattern transition process is also explicitly verified by the waved variations of MVN, MSN, and IEN in Fig. 9.

A careful observation on Fig. 9(a) and 9(c) finds that the wave of MVN or IEN presents discontinuous property. This suggests that there may be some kind of subtle structures existing locally. Figure 10 shows the pattern transition in a tiny range [4.27384, 4.27389]. All the patterns exhibit similar configuration, but the pattern structures fluctuate during

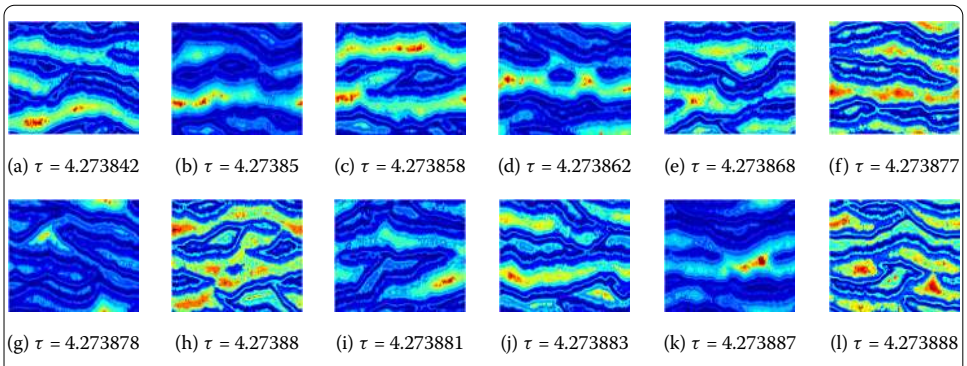

(a) $\tau = 4.273842$ (b) $\tau = 4.27385$ (c) $\tau = 4.273858$ (d) $\tau = 4.273862$ (e) $\tau = 4.273868$ (f) $\tau = 4.273877$

(g) $\tau = 4.273878$ (h) $\tau = 4.27388$ (i) $\tau = 4.273881$ (j) $\tau = 4.273883$ (k) $\tau = 4.273887$ (l) $\tau = 4.273888$

Figure 10 Pattern transition with the variation of τ covering [4.27384, 4.27389]. In this range, all the patterns exhibit similar configuration but the pattern structures fluctuate. The conditions for pattern simulations are exactly the same as those in Fig. 3

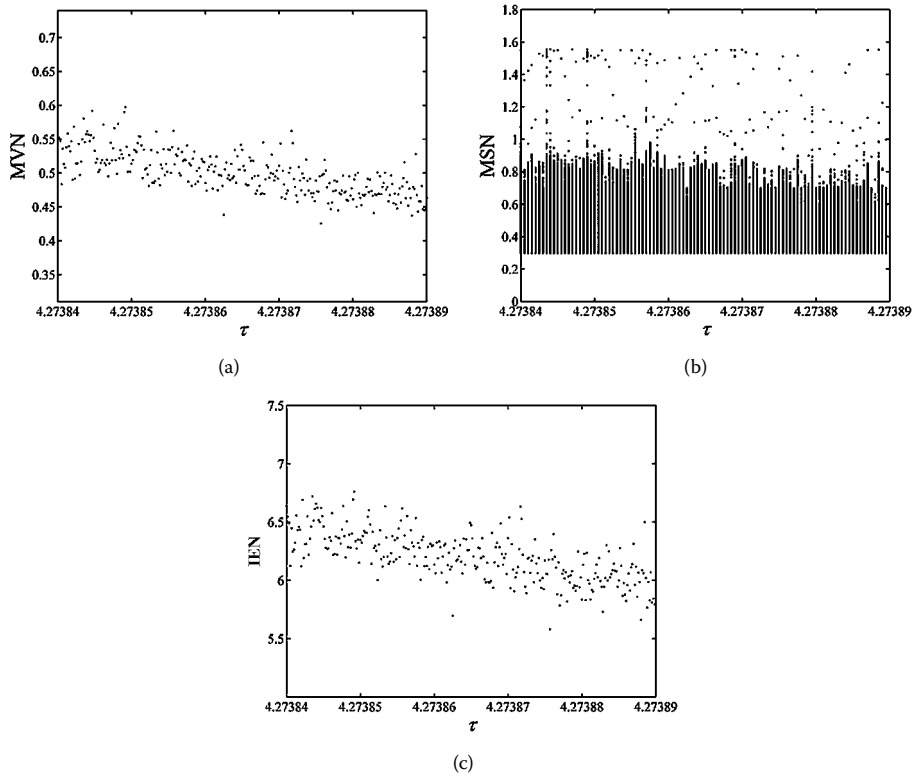

Figure 11 Graphs of (**a**) MVN, (**b**) MSN, and (**c**) IEN corresponding to Fig. 10, demonstrating stochastic pattern fluctuation in the pattern transition

the entire range. To quantitatively determine the nonlinear characteristics of the pattern transition in the range, the graphs of MVN, MSN, and IEN are also plotted. Figure 11 explicitly demonstrates stochastic pattern fluctuation, which emerges based on a common background with the main states of $N(i,j)$ ranging about in $[0.3, 0.8]$ (Fig. 11(b)). This explains similarity and variation of the patterns in the range $[4.27384, 4.27389]$. Moreover, the pattern fluctuation presents the property of self-similarity when the τ value varies in

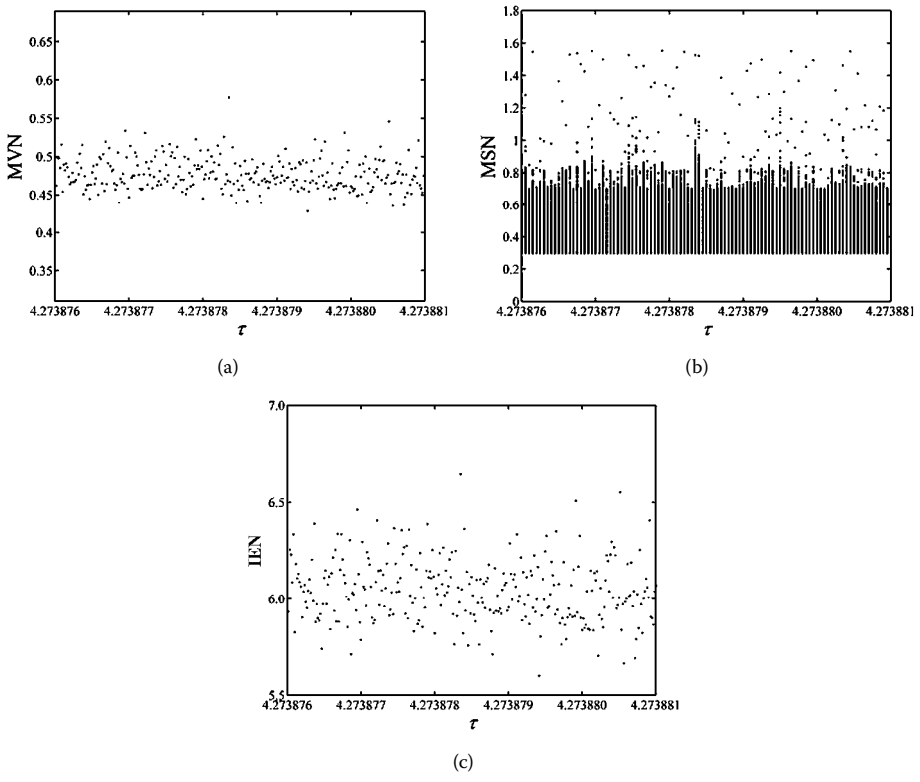

Figure 12 Graphs of (**a**) MVN, (**b**) MSN, and (**c**) IEN corresponding to the pattern transition with the variation of τ covering [4.273876, 4.273881], suggesting a property of self-similarity in the pattern fluctuation. The conditions for pattern simulations are exactly the same as those in Fig. 3

the level of 10^{-5} or below (Figs. 11 and 12). This may be essential regularity for the pattern variations in tiny parameter ranges.

5 Discussion and conclusion

For predator–prey systems, self-organization of ordered patterns, resulting from spatial symmetry breaking induced by Turing instability, also plays a key role in revealing and explaining regular population distribution involved in predation relationship. Previously, research works have been focused upon how the pattern self-organization takes place under Turing instability conditions. A great deal of research works demonstrated that Turing instability can generate diverse and complex patterns in the predator–prey systems [3, 12, 25, 32], and [31]. Particularly, Hopf–Turing instability induces spatial symmetry breaking at homogeneous oscillating states and leads to the formation of oscillatory patterns, where the dynamics of predator and prey is always varying spatially and temporally [12] and [31]. A few research works even found that the Hopf–Turing instability can produce patterns with spatiotemporal chaos, which plays a vital role in the spatiotemporal organization of ecological systems [13] and [35].

When the Turing instability occurs on the routes to chaos, the discrete system can exhibit surprising spatiotemporal complexity. Nevertheless, the study on pattern self-organization and pattern transition on the route to chaos is still seldom documented in the literature. Huang and Zhang [24] investigated the pattern transition along the routes to chaos induced by flip bifurcation and Hopf bifurcation, finding a transition from ordered

spiral patterns, through spiral fragmentation, to spatiotemporal chaos with complete disorder. Such a transition process accords with the dynamic variation on the route to chaos. Kaneko studied the pattern formation on the transition route from torus to chaos, revealing rich spatiotemporal dynamics such as frozen random pattern, Brownian motion of defect, defect turbulence, pattern competition intermittency, fully developed turbulence, and so on [36]. Compared with former research works, the present approach also finds rich spatiotemporal dynamics and some new nonlinear characteristics for the discrete predator–prey systems. The following concluding remarks can be summarized.

(1) Hopf bifurcation starts a route to chaos, on which the predator–prey dynamics experiences transition from an invariant closed curve, to complex invariant cycles, and finally to chaotic attractors, with periodic windows repeatedly occurringin-between. The dynamic variation on the route to chaos demonstrates a transition from ordered states to disordered states.
(2) Hopf–Turing instability occurring on the route to chaos leads to self-organization of diverse patterns. Ordered patterns of stripes, bands, circles, and various disordered states are revealed. Moreover, tiny variation of parameter value can result in two different patterns, reflecting pattern diversity on the route to chaos.
(3) When the information entropy of patterns shows high values, rich self-organized patterns may be indicated.
(4) Complex pattern transition takes place on the route to chaos. When we zoom in to observe the pattern transition in smaller and smaller parameter ranges, subtle structures for transition process can be found.
(5) Alternation between self-organized structured patterns and disordered patterns emerges as the main nonlinear characteristic for pattern transition. Such alternation reveals that ordered patterns and disordered states can keep in continuous transition from one to the other in the discrete system.
(6) When the value of parameter τ varies in the level from 10^{-3} to 10^{-4}, cyclic pattern transition process occurs repeatedly. Such a dynamical phenomenon can be explicitly verified by waved variations of the entropy of patterns.
(7) When the value of parameter τ varies in the level of 10^{-5} or below, stochastic pattern fluctuation dominates the pattern transition. Moreover, the pattern fluctuation presents a property of self-similarity, reflecting basic regularity for pattern variations in tiny parameter ranges.

Acknowledgements
The authors would like to acknowledge with great gratitude the support of the National Major Science and Technology Program for Water Pollution Control and Treatment (No. 2017ZX07101-002, No. 2015ZX07203-011), the Fundamental Research Funds for the Central Universities (No. JB2017069).

Competing interests
The authors have no financial and non-financial competing interests for this research work.

Authors' contributions
The authors' contributions are described as follows. HZ provided the innovations for the work, TH and XC wrote and modified the paper together, SM checked the calculations for bifurcation analysis and gave suggestions for paper writing, and GP helped to perform numerical simulations. All authors read and approved the final manuscript.

Publisher's Note

Received: 30 October 2017 Accepted: 11 April 2018 Published online: 09 May 2018

References

1. Cross, M., Greenside, H.: Pattern Formation and Dynamics in Nonequilibrium Systems. Cambridge University Press, Cambridge (2009)
2. Nicolis, G., Progogine, I.: Exploring Complexity: An Introduction. Freeman, San Francisco (1989)
3. Kondo, S., Miura, T.: Reaction-diffusion model as a framework for understanding biological pattern formation. Science **329**, 1616–1620 (2010)
4. Walgraef, D.: Spatio-Temporal Pattern Formation: With Examples from Physics, Chemistry, and Materials Science. Springer, New York (2012)
5. Levin, S.A.: Pattern formation in ecological communities. In: Steele, J.S. (ed.) Spatial Pattern in Plankton Communities, pp. 433–465. Plenum, New York (1978)
6. Rietkerk, M., Van de Koppel, J.: Regular pattern formation in real ecosystems. Trends Ecol. Evol. **23**(3), 169–175 (2008)
7. Blasius, B., Huppert, A., Stone, L.: Complex dynamics and phase synchronization in spatially extended ecological systems. Nature **399**(6734), 354–359 (1999)
8. Rietkerk, M., Dekker, S.C., de Ruiter, P.C., van de Koppel, J.: Self-organized patchiness and catastrophic shifts in ecosystems. Science **305**(5692), 1926–1929 (2004)
9. Valentin, C., d'Herbès, J.M., Poesen, J.: Soil and water components of banded vegetation patterns. Catena **37**(1), 1–24 (1999)
10. Bascompte, J., Solé, R.V.: Rethinking complexity: modelling spatiotemporal dynamics in ecology. Trends Ecol. Evol. **10**(9), 361–366 (1995)
11. Van den Broeck, C., Parrondo, J.M.R., Toral, R.: Noise-induced nonequilibrium phase transition. Phys. Rev. Lett. **73**(25), 3395 (1994)
12. Huang, T., Zhang, H., Yang, H., Wang, N., Zhang, F.: Complex patterns in a space- and time-discrete predator–prey model with Beddington–DeAngelis functional response. Commun. Nonlinear Sci. Numer. Simul. **43**, 182–199 (2017)
13. Rodrigues, L.A.D., Mistro, D.C., Petrovskii, S.: Pattern formation in a space- and time-discrete predator–prey system with a strong Allee effect. Theor. Ecol. **5**, 341–362 (2012)
14. May, R.M.: Simple mathematical models with very complicated dynamics. Nature **261**, 459–467 (1976)
15. Segel, L.A., Jackson, J.L.: Dissipative structure: an explanation and an ecological example. J. Theor. Biol. **37**(3), 545–559 (1972)
16. Gierer, A., Meinhardt, H.: A theory of biological pattern formation. Kybernetik **12**(1), 30–39 (1972)
17. Levin, S.A., Segel, L.A.: Hypothesis for origin of planktonic patchiness. Nature **259**, 659 (1976)
18. Huang, T., Zhang, H., Yang, H.: Spatiotemporal complexity of a discrete space-time predator–prey system with self- and cross-diffusion. Appl. Math. Model. **47**, 637–655 (2017)
19. Wang, C.: Rich dynamics of a predator–prey model with spatial motion. Appl. Math. Comput. **260**, 1–9 (2015)
20. Sun, G.Q., Zhang, J., Song, L.P., Jin, Z., Li, B.L.: Pattern formation of a spatial predator–prey system. Appl. Math. Comput. **218**, 11151–11162 (2012)
21. Sun, G.Q., Jin, Z., Liu, Q.X., Li, L.: Dynamical complexity of a spatial predator–prey model with migration. Ecol. Model. **219**, 248–255 (2008)
22. Liu, P.P.: An analysis of a predator–prey model with both diffusion and migration. Math. Comput. Model. **51**, 1064–1070 (2010)
23. Petrovskii, S., Li, B.L.: An exactly solvable model of population dynamics with density-dependent migrations and the Allee effect. Math. Biosci. **186**, 79–91 (2003)
24. Huang, T., Zhang, H.: Bifurcation, chaos and pattern formation in a space- and time-discrete predator–prey system. Chaos Solitons Fractals **91**, 92–107 (2016)
25. Mistro, D.C., Rodrigues, L.A.D., Petrovskii, S.: Spatiotemporal complexity of biological invasion in a space- and time-discrete predator–prey system with the strong Allee effect. Ecol. Complex. **9**, 16–32 (2012)
26. Punithan, D., Kim, D.K., McKay, R.I.B.: Spatio-temporal dynamics and quantification of daisyworld in two-dimensional coupled map lattices. Ecol. Complex. **12**, 43–57 (2012)
27. Liu, X., Xiao, D.: Complex dynamic behaviors of a discrete-time predator–prey system. Chaos Solitons Fractals **32**, 80–94 (2007)
28. Jing, Z., Yang, J.: Bifurcation and chaos in discrete-time predator–prey system. Chaos Solitons Fractals **27**, 259–277 (2006)
29. Antal, T., Droz, M.: Phase transitions and oscillations in a lattice prey–predator model. Phys. Rev. E **63**, 056119 (2001)
30. Schaffer, W.M.: Order and chaos in ecological systems. Ecology **66**, 93–106 (1985)
31. Haque, M.: Existence of complex patterns in the Beddington–DeAngelis predator–prey model. Math. Biosci. **239**, 179–190 (2012)
32. Zhang, X.C., Sun, G.Q., Jin, Z.: Spatial dynamics in a predator–prey model with Beddington–DeAngelis functional response. Phys. Rev. E **85**, 021924 (2012)
33. Bai, L., Zhang, G.: Nontrivial solutions for a nonlinear discrete elliptic equation with periodic boundary conditions. Appl. Math. Comput. **210**, 321–333 (2009)
34. Han, Y.-T., Han, B., Zhang, L., Xu, L., Li, M.-F., Zhang, G.: Turing instability and wave patterns for a symmetric discrete competitive Lotka–Volterra system. WSEAS Trans. Math. **10**, 181–189 (2011)
35. Medvinsky, A.B., Petrovskii, S.V., Tikhonova, I.A., Malchow, H., Li, B.: Spatiotemporal complexity of plankton and fish dynamics. SIAM Rev. **44**, 311–370 (2002)
36. Kaneko, K.: Pattern dynamics in spatiotemporal chaos: pattern selection, diffusion of defect and pattern competition intermittency. Phys. D, Nonlinear Phenom. **34**, 1–41 (1989)